
Global-correlated 3D-decoupling Transformer for Clothed Avatar Reconstruction

Zechuan Zhang¹, Li Sun¹, Zongxin Yang¹, Ling Chen², Yi Yang^{1†}

¹ ReLER, CCAI, Zhejiang University

² AAII, University of Technology Sydney

Abstract

Reconstructing 3D clothed avatars from single images is a challenging task, especially when encountering complex poses and loose clothing. Current methods exhibit limitations in performance, largely attributable to their dependence on insufficient 2D image features and inconsistent query methods. Owing to this, we present **Global-correlated 3D-decoupling Transformer** for clothed Avatar reconstruction (**GTA**), a novel transformer-based architecture that reconstructs clothed human avatars from monocular images. Our approach leverages transformer architectures by utilizing a Vision Transformer model as an encoder for capturing global-correlated image features. Subsequently, our innovative 3D-decoupling decoder employs cross-attention to decouple tri-plane features, using learnable embeddings as queries for cross-plane generation. To effectively enhance feature fusion with the tri-plane 3D feature and human body prior, we propose a hybrid prior fusion strategy combining spatial and prior-enhanced queries, leveraging the benefits of spatial localization and human body prior knowledge. Comprehensive experiments on CAPE and THuman2.0 datasets illustrate that our method outperforms state-of-the-art approaches in both geometry and texture reconstruction, exhibiting high robustness to challenging poses and loose clothing, and producing higher-resolution textures. Codes are available at <https://github.com/River-Zhang/GTA>.

1 Introduction

As virtual worlds and metaverse technology gain popularity, the demand for advanced techniques to reconstruct 3D clothed human avatars from single images is rapidly increasing. These techniques [1, 2, 3, 4, 5, 6, 7, 8, 9] are employed across various areas, such as AR/VR, social telepresence, virtual try-on, or the movie industry. However, in-the-wild images often present challenges, such as loose clothing and complex poses, which are not typically found in training data. As a result, there is a pressing need for models that can effectively generalize to these scenarios and reconstruct accurate, animatable, and high-resolution 3D human avatars.

In light of the significant progress made in 3D clothed human avatar reconstruction, existing models still face two main limitations: (i) **Overreliance on 2D image features**. Sole dependence on 2D CNN-based features compromises the accuracy of 3D object reconstructions due to the lack of global correlation. Despite the integration of 3D features from human body priors in methods like [3, 2, 7, 10], their inconsistent performance with loose clothing and challenging poses (See Fig. 2) indicates insufficient integration. Additionally, optimization-based methods [4, 11, 12, 13] can be complex and prone to errors, reducing reliability. (ii) **Inconsistent query methods**. Current strategies for querying features differ and have drawbacks. The pixel-aligned method [1, 6] directly

†: the corresponding author.



Figure 1: Given a monocular image as input, GTA reconstructs the full 3D geometry and texture of the subject portrayed, allowing for various applications such as virtual try-on and animation.

projects query points on feature maps but lacks guidance from human body prior, while the prior-guided strategy [7] integrates features on a human body prior but may lead to loss of detailed information on the image and result in 3D avatar reconstructions with an increased level of fuzziness.

Considering the limitations discussed above, we propose that 2D feature maps are insufficient for 3D reconstruction tasks, while global-correlated 3D feature representations offer a more effective solution. Traditional 3D representations are space-intensive and inefficient, necessitating alternatives such as the memory-conserving tri-plane representation [14]. However, generating global-correlated 3D representations from monocular images remains challenging due to difficulties in obtaining orthogonal plane feature maps. Our approach employs learnable embeddings and cross-attention mechanisms to effectively model intricate cross-plane relationships, enabling robust and precise 3D feature extraction. Furthermore, it is important to develop a strategy that synergizes various query methods while maintaining simplicity and efficiency. By combining existing strategies for 3D features, our method leverages localized spatial features and prior knowledge of human body structure, resulting in a balanced feature extraction process that improves reconstruction performance.

In response to the identified challenges, we present **GTA** (Global-correlated 3D-decoupling Transformer for clothed Avatar reconstruction), employing a novel global-correlated 3D-decoupling transformer and a hybrid prior fusion strategy for comprehensive 3D geometry and texture reconstruction. Our vision transformer-based encoder extracts global-correlated features from the input image, while our unique 3D-decoupling decoder disentangles tri-plane 3D features using learnable embeddings as queries. This integration of global-correlated encoding and 3D-decoupling decoding effectively captures the 3D avatar structure from a single image. To further enhance feature fusion, our hybrid prior fusion strategy combines spatial and prior-enhanced queries, leveraging the benefits of spatial localization and human body prior knowledge. This efficient and accurate integration strategy achieves state-of-the-art performance in single-view human avatar reconstruction.

Our proposed model, trained on THuman2.0 [15], outperforms state-of-the-art(SOTA) methods in geometry and texture reconstruction. We achieve a significant reduction in Chamfer distance on CAPE-FP [16] test dataset, below 0.8cm for the first time, and demonstrate superior side-view normal performance, illustrating our method’s efficacy in reconstructing accurate 3D clothed human avatars. Our model excels in handling complex poses and loose clothing, and attains state-of-the-art texture reconstruction with higher PSNR scores. Moreover, it can be extended to animation and virtual try-on applications, showcasing its wide-ranging real-world potential. Our main contributions include:

- We introduce a novel global-correlated 3D-decoupling transformer that effectively disentangles tri-plane features, thereby substantially enhancing the reconstruction of clothed avatars from 2D images. To the best of our knowledge, our approach is the pioneering application of transformers in 3D feature decoupling for monocular human avatar reconstruction tasks.
- We put forward an innovative hybrid prior fusion strategy for feature query, combining spatial query’s localization capabilities with prior-enhanced query’s ability to incorporate knowledge of the human body prior, ultimately leading to improved geometry and texture reconstruction performance.
- Our proposed model achieves state-of-the-art performance in both clothed human geometry and texture reconstruction, outperforming previous models and exhibiting enhanced side-view normal performance.



Figure 2: GTA vs. SOTA. SOTA methods (red) are vulnerable to challenging poses and loose clothing, leading to artifacts such as non-human shapes (PIFu [1], PaMIR [3]), incomplete clothing reconstruction (ICON [2]), and erroneous stitching (ECON [4]). GTA deals with these challenges and produces high-quality results (blue).

2 Related Work

Monocular Human Reconstruction has been an active area of research for many years. This task is inherently ill-posed due to the lack of 3D information, requiring additional assumptions or prior knowledge to recover the full 3D structure. Previous research has proposed effective parametric human prior models [17, 18, 19, 20, 21], which employs statistical methods to reduce the variations in human body shape and pose to a compact set of parameters. By leveraging this model, subsequent research has proposed novel methods to estimate or regress the model parameters from a single RGB image [22, 23, 24, 25, 26]. However, the human prior models can only capture a minimally clothed body without complex details like garments, adornments, or hairstyles. To address this limitation, some researchers add offsets on the top of prior body vertices to simulate outfits [27, 28, 29, 30, 31]. While these methods can effectively represent clothing close to the body surface and use blending weights of surface vertices to drive the clothing, they are not suitable for geometry topology far from the human body, such as robes and dresses.

In order to overcome the constraints imposed on reconstruction by clothing shape and type, researchers have explored various alternative representations for the human body, including voxels [32, 33], visual hulls [34], double depth maps [11, 12, 13, 4], and UV maps translation [35]. Among these diverse methods, implicit function-based methods [36] have shown the most remarkable performance. Saito et al. introduced PIFu [1], which firstly incorporates implicit functions into the problem of human body reconstruction. The method leverages a CNN-based neural network to extract features from 2D images and uses implicit functions to express the spatial geometry field, such as signed distance functions (SDF) [37] and occupancy fields [38]. While implicit function-based methods [1, 39, 6] can accurately reconstruct the complex topology of clothed human body surfaces, they may generate non-anatomical shapes for out-of-distribution poses due to the lack of regularization.

To improve pose robustness, recent research [3, 2, 4, 5, 7] has utilized the prior knowledge to guide implicit function representation. These methods have shown promising results in enhancing the quality and accuracy of reconstruction geometry, particularly for challenging poses. However, these methods, like previous ones, still rely on 2D features extracted from CNN-based networks, even though some of them incorporate 3D features obtained from human body prior. In the reconstruction process, the feature obtained by 2D projection may result in incomplete reconstructions from other viewpoints and diminish overall reconstruction accuracy. Our method extracts global-correlated 3D-aware feature to efficiently represent the clothed human avatar.

Transformers in Vision. The transformer architecture, initially proposed by Vaswani et al. [40], has achieved immense success across domains like NLP, speech recognition, and multimodal applications. Inspired by this, many studies have attempted to adapt the transformer architecture to the field of computer vision. Among these explorations, the Vision Transformer (ViT) proposed by Dosovitskiy et al. [41] has shown impressive performance in 2D visual tasks. Meanwhile, transformer’s ability to model global and long-range correlation is also suitable for 3D vision tasks. Therefore, we leverage a ViT-based 3D transformer with cross-plane attention to efficiently extract global-correlated 3D features for better human reconstruction.

Generative 3D-aware Feature. Recent studies [14] have proposed the tri-plane 3D feature representation method, which efficiently extracts features from objects in three orthogonal orientations. Tri-plane representation has been demonstrated high efficacy in generating 3D objects [42], particu-

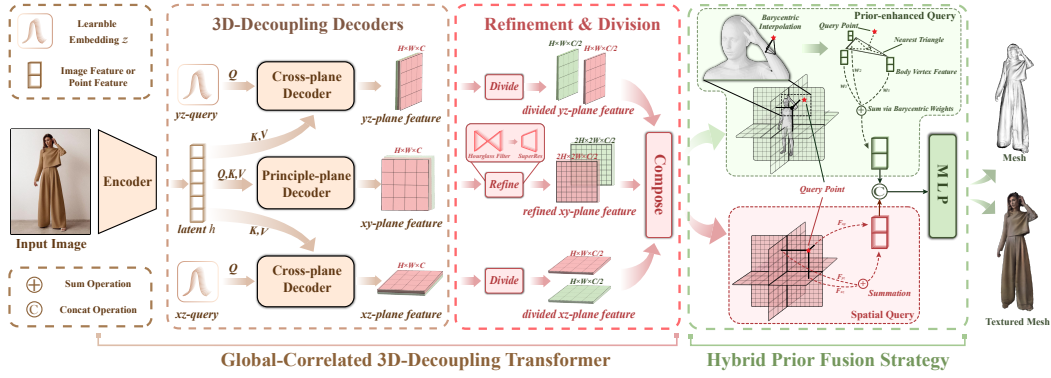


Figure 3: GTA Overview. GTA has two key modules: (1) the global-correlated 3D-decoupling transformer and (2) the hybrid prior fusion strategy. The former module extracts a latent h from the input image and integrates it with learnable embeddings z via 3D-decoupling decoders, producing disentangled tri-plane features. The latter module employs spatial (red) and prior-enhanced (green) queries to merge features from the two tri-planes, thus enabling geometry and texture reconstruction.

larly 3D human bodies [43, 44, 45]. Thus, the tri-plane representation method holds potential for application in human body reconstruction. Nevertheless, the challenge of establishing a reasonable relationship between the input monocular image and the three planes of features remains an unresolved problem. In our method, we introduce learnable embeddings to represent features of spatial planes that are not directly visible, and utilize cross-attention mechanisms to establish relationships between the input image and other planes.

3 Method

We introduce an implicit function-based framework for reconstructing 3D clothed human models from a single image (See Fig. 3). Our model employs a global-correlated 3D-decoupling transformer to disentangle tri-plane features and harnesses a hybrid prior fusion strategy for reconstructing the full 3D geometry and texture of the clothed avatar. In the following sections, we will discuss the preliminaries of GTA in Sec. 3.1, the global-correlated 3D-decoupling transformer in Sec. 3.2, and the hybrid prior fusion strategy in Sec. 3.3.

3.1 Preliminary

SMPL. The Skinned Multi-Person Linear (SMPL) model [18] is a widely-used parametric human body model. The SMPL model utilizes shape parameters $\beta \in \mathbb{R}^{10}$ and pose parameters $\theta \in \mathbb{R}^{3 \times K}$ to parameterize the deformation of the human body mesh \mathcal{M} :

$$\mathcal{M}(\beta, \theta) : \beta \times \theta \mapsto \mathbb{R}^{3 \times N} \quad (1)$$

where $K = 24$ joints and $N = 6890$ vertices. Shape parameter β describes the body's overall size and proportions and pose parameter θ defines the positions and orientations of the joints relative to their default positions. SMPL enables effective representation and manipulation of human body shape and pose in various applications.

Implicit Function. Implicit function is a powerful tool for modeling complex geometries with neural networks. Our implicit function maps an input point to a scalar value that represents the spatial field including occupancy field and color field. The occupancy field takes a point in space as input and outputs a binary value indicating whether the point is inside or outside the human surface. Our reconstructed human surface can be represented as $\mathcal{S}_{\mathcal{I}\mathcal{F}}$:

$$\mathcal{S}_{\mathcal{I}\mathcal{F}} = \{x \in \mathbb{R}^3 \mid \mathcal{I}\mathcal{F}(x) = (o, c)\} \quad (2)$$

where occupancy $o = 0.5$, color $c \in \mathbb{R}^3$, and $\mathcal{I}\mathcal{F}$ represents the implicit function.

3.2 Global-correlated 3D-decoupling Transformer

Directly extracting 3D information from a single 2D image is not feasible, this is largely due to the fact that 3D features include information from planes orthogonal with the image plane (also noted as xy -plane, principle-plane). To effectively decouple cross-plane features from a monocular image input, it is crucial to have additional guiding information. This is where the idea of learnable embeddings and the use of a cross-attention mechanism prove valuable. Inspired by this, we devise a novel transformer-based architecture including a global-correlated encoder and a 3D-decoupling decoder to disentangle 3D features from single input images.

Global-correlated Encoder. In our method, we employ a vision transformer to encode the input image and capture global correlations in the image, resulting in high-dimensional global-correlated image features. Our encoder module processes the input image by dividing it into non-overlapping $n \times n$ patches and subsequently mapping them to image features through transformer blocks. This procedure generates a latent \mathbf{h} for a image I .

3D-decoupling Decoder. To decode 3D tri-plane features from the encoder output, we propose to use two types of decoders: the principle-plane decoder and the cross-plane decoder. Our principle-plane decoder generates xy -plane features, which share the same plane as the input image. This decoder effectively reverses the encoding operation, leveraging a self-attention mechanism on the encoder output and converting the image features into a principal feature map $F_{xy} \in \mathbb{R}^{H \times W \times C}$.

In order to generate plane features orthogonal with the principle plane while preserving global correlation with the principle plane, we employ the cross-plane decoder to decode yz and xz plane features from input image features. To guide the decoder in decoding features from different planes, we introduce a learnable embedding \mathbf{z} that supplies additional information for decoupling new planes. The learnable embedding \mathbf{z} is first processed through self-attention encoding. It is then used as a query in a multi-head cross-attention mechanism with the output image latent \mathbf{h} from the encoder stack. The image features are converted into keys and values for the cross-attention mechanism,

$$\text{CrossAttn}(\mathbf{z}, \mathbf{h}) = \text{Softmax}\left(\frac{(W^Q \text{SelfAttn}(\mathbf{z}))(W^K \mathbf{h})^T}{\sqrt{d}}\right)(W^V \mathbf{h}) \quad (3)$$

where W^Q , W^K , and W^V are learnable parameters and d is the scaling coefficient. Following the original transformer architecture [40], our model employs residual connections [46] and layer normalization [47] after each sub-layer. The entire decoder consists of multiple identical layers, and we use two such decoders to produce feature maps $F_{yz} \in \mathbb{R}^{H \times W \times C}$ and $F_{xz} \in \mathbb{R}^{H \times W \times C}$.

Principle-plane Refinement. In accordance with the approach demonstrated in [6], higher-resolution feature maps play a crucial role in producing detailed geometry and sharper textures. Hence, we use both the original image and the principle-plane feature map, to produce a higher-resolution feature map. The original image is initially down-convoluted to match the principle-plane size and then concatenated along the channel dimension. Subsequently, they are fed into a streamlined Hourglass network and a super-resolution module for refinement. This process generates a higher-resolution feature map $F_{xy}^{refine} \in \mathbb{R}^{2H \times 2W \times C}$.

$$F_{xy}^{refine} = \text{SuperRes}(\text{Hourglass}(\text{DownConv}(I) \odot F_{xy})) \quad (4)$$

where \odot means concatenation operation. The resulting xy plane (principle-plane) exhibits a higher resolution than the yz and xz planes and incorporates more information from the original image, leading to higher fidelity reconstruction.

Tri-plane Division. After obtaining each plane, we evenly divide the plane features along the channel dimension into two groups, creating two tri-planes. For one group, we perform a spatial query to acquire features for query points, while for the other group, we utilize a prior-enhanced query to integrate the human body prior. Please refer to the next section for a detailed introduction to our novel hybrid prior fusion strategy.



Figure 4: Qualitative 3D human reconstruction for real images showcasing diverse poses and clothing variations. For each example, we show the input image along with two views of the reconstructed geometry and front view of the reconstructed texture. Our approach is robust to challenging poses and loose clothing, and contains detailed geometry and texture. See Sec. E for more results.

3.3 Hybrid Prior Fusion Strategy

In previous works, two primary methods have been utilized for acquiring query point features, each with significant limitations as previously discussed in Sec. 1. To address this, we propose a hybrid prior fusion strategy that combines the strengths of both spatial query and prior-enhanced query.

Spatial Query. Following [14], we extend the pixel-aligned query into 3D space, denoted as spatial query. This method projects query points onto the xy , yz , and xz planes of a tri-plane group, producing localized features that capture important details for reconstruction. We combine the F_{yz} and F_{xz} features by summation and concatenate the result with F_{xy}^{refine} to generate the spatial query feature $F_{SQ}(\mathbf{x})$:

$$F^{SQ}(\mathbf{x}) = F_{xy}^{SQ}(\mathbf{x}) \odot (F_{yz}^{SQ}(\mathbf{x}) + F_{xz}^{SQ}(\mathbf{x})) \quad (5)$$

where $F_{xy}^{SQ}(\mathbf{x})$, $F_{yz}^{SQ}(\mathbf{x})$, $F_{xz}^{SQ}(\mathbf{x})$ are extracted from F_{xy}^{refine} , F_{yz} , F_{xz} , and \odot is concatenation.

Prior-enhanced Query. For the other tri-plane, we project the human body prior [18, 19] mesh vertices onto the three planes similar to the spatial query above to obtain the feature $F^{PQ}(\mathbf{v})$, $\mathbf{v} \in \mathcal{M}$, where \mathcal{M} is the body prior mesh. For each query point \mathbf{x} , we find the nearest triangular face $t_{\mathbf{x}} = [\mathbf{v}_0, \mathbf{v}_1, \mathbf{v}_2] \in \mathbb{R}^{3 \times 3}$ and use barycentric interpolation to integrate features for \mathbf{x} (See Fig. 3), denoted as $F_{PQ}(\mathbf{x})$:

$$F^{PQ}(\mathbf{x}) = uF^{PQ}(\mathbf{v}_0) + vF^{PQ}(\mathbf{v}_1) + wF^{PQ}(\mathbf{v}_2) \quad (6)$$

where $[u, v, w]$ represents the barycentric coordinates of the query point \mathbf{x} projected onto triangle $t_{\mathbf{x}}$.

Hybrid Prior Fusion Strategy. Spatial query projects the query points directly onto tri-plane features, providing detailed information but lacking prior knowledge. On the other hand, the prior-enhanced query merges body prior information but may cause an increased level of fuzziness. Therefore, we concatenate these two query features to capitalize on each method's strengths and compensate for their weaknesses. Furthermore, we also include the signed distance between query point and human prior mesh $\mathcal{SDF}_{Prior}(\mathbf{x})$ and pixel-aligned normal feature $F_N(\mathbf{x})$ as input to the implicit function for predicting occupancy and color. Consequently, the reconstructed human surface $\mathcal{S}_{\mathcal{I}\mathcal{F}}$ can be represented as:

Table 1: Quantitative comparison on geometry against other methods. *: obtained from [2, 4].

Method	Training Data	CAPE-NFP [16]			CAPE-FP [16]			THuman2.0 [15]		
		Chamfer ↓	P2S↓	Normals↓	Chamfer ↓	P2S↓	Normals↓	Chamfer ↓	P2S↓	Normals↓
PIFu [1]	THuman2.0 [15]	2.458	2.117	0.094	1.786	1.639	0.071	1.586	1.530	0.088
PIFu* [1]	Renderpeople [48]	2.973	2.940	0.111	2.100	2.093	0.091	-	-	-
PIFuHD* [6]	Renderpeople [48]	3.767	3.591	0.123	2.302	2.335	0.090	-	-	-
PaMIR [3]	THuman2.0 [15]	1.603	1.429	0.068	1.502	1.291	0.064	1.276	1.247	0.080
PaMIR* [3]	Renderpeople [48]	1.413	1.321	0.063	1.225	1.206	0.055	-	-	-
ICON [2]	THuman2.0 [15]	1.096	1.085	0.046	0.969	0.987	0.041	1.249	1.368	0.076
ICON* [2]	Renderpeople [48]	1.070	1.013	0.059	1.202	1.170	0.055	-	-	-
ECON [4]	THuman2.0 [15]	0.942	0.933	0.035	0.904	0.894	0.033	2.120	1.807	0.074
ECON* [4]	THuman2.0 [15]	0.926	0.917	0.037	-	-	-	-	-	-
Ours	THuman2.0 [15]	0.911	0.917	0.042	0.763	0.763	0.035	0.814	0.862	0.055

$$\mathcal{S}_{\mathcal{IF}} = \{\mathbf{x} \in \mathbb{R}^3 \mid \mathcal{IF}(F^{SQ}(\mathbf{x}), F^{PQ}(\mathbf{x}), \mathcal{SF}_{Prior}(\mathbf{x}), F_N(\mathbf{x})) = (o, \mathbf{c})\} \quad (7)$$

where occupancy $o = 0.5$, color $\mathbf{c} \in \mathbb{R}^3$, and \mathcal{IF} represents the implicit function.

Training Objectives. For each 3D scan, we consider two sets of points as training data, denoted as G_o and G_c . G_c is sampled uniformly with a slight perturbation along the normals of the mesh surface, whereas G_o is sampled according to the same strategy as in PIFu [1], where points are sampled near the mesh surface and throughout the entire space.

For the points in G_o , we employ the following loss function:

$$\mathcal{L}_o = \frac{1}{|G_o|} \sum_{\mathbf{x} \in G_o} BCE(\hat{o}_{\mathbf{x}} - o_{\mathbf{x}}) \quad (8)$$

where $\hat{o}_{\mathbf{x}}$ denotes the model’s predicted occupancy, while $o_{\mathbf{x}}$ signifies the ground truth occupancy. For the sampled points in G_c , we apply the following loss function:

$$\mathcal{L}_c = \frac{1}{|G_c|} \sum_{\mathbf{x} \in G_c} |\hat{\mathbf{c}}_{\mathbf{x}} - \mathbf{c}_{\mathbf{x}}| \quad (9)$$

where $\hat{\mathbf{c}}_{\mathbf{x}}$ represents the predicted color at location \mathbf{x} by the model, while $\mathbf{c}_{\mathbf{x}}$ indicates the true color of the mesh at \mathbf{x} . The overall loss function is expressed by:

$$\mathcal{L}_{GTA} = \mathcal{L}_o + \mathcal{L}_c \quad (10)$$

4 Experiments

Strategy for Point Sampling. In the context of each training subject, our approach involves obtaining 2048 points for occupancy, denoted as G_o , and 2048 points for color, symbolized as G_c . The method for occupancy point sampling is aligned with the strategy illustrated in [1]. Color points are sampled uniformly, with a minor Gaussian disturbance, expressed as $\mathcal{N}(0, \sigma)$, wherein our experiment σ is set at 0.1 cm. This disturbance occurs along the normals of the mesh surface. We obtain labels for the ground truth geometry, which specify whether a point is inside or outside the surface, through the application of Kaolin [49] to ascertain if a point lies within the ground truth mesh. The source of the ground truth color labels is the UV texture map of the 3D meshes.

Model Structure. To generate global-correlated latent features, we utilize a Vision Transformer (ViT) [41] model of depth 6, functioning as our global-correlated encoder, and generating an output of size 1024×256 . Our 3D-decoupling decoder incorporates both cross-plane and principal-plane decoders, each with a depth of three. The cross-plane decoder is initialized with learnable embeddings that experience a Gaussian perturbation to align cohesively with the encoder’s output shape. The configuration of the cross-plane decoder corresponds with the structure described in [40], while the principal-plane decoder emulates the global-correlated encoder. Each decoder outputs a feature map $F \in \mathbb{R}^{128 \times 128 \times 64}$. During refinement, a 2-stack hourglass and a transpose convolution module are integrated to generate a higher resolution principal-plane feature map $F_{xy}^{refine} \in \mathbb{R}^{128 \times 128 \times 64}$. Following the feature acquisition through our hybrid prior fusion method, two identical Multilayer

Perceptrons (MLPs) are employed for separate predictions of occupancy and color, each with layer sizes of [512, 1024, 512, 256, 128, 1]. In the inference phase, we utilize Rembg [50] for background subtraction in in-the-wild images. The Marching Cubes algorithm [51] is employed for generating 3D meshes, while off-the-shelf models from ICON [2] are leveraged for the production of normal maps. This normal map is further processed through a 2-stack hourglass to achieve a size of $128 \times 128 \times 6$. Besides the front/back normal maps are also used as input into the encoder with the image. The model, implemented in PyTorch Lightning [52], is trained for 10 epochs with a learning rate of 1e-4 and a batch size of 4, over a span of 2 days on a single NVIDIA GeForce RTX 3090 GPU.

Datasets. Our model was trained on the THuman2.0 [15], featuring 526 high-quality human scans, with 505 designated for training and 21 for evaluation. Testing was primarily conducted on the CAPE [16] and THuman2.0, with the former divided into "CAPE-FP" and "CAPE-NFP" subsets to examine model generalization on different pose types. Further dataset and implementation details are available in Sec. A.

Metrics. We employ Chamfer and point-to-surface (P2S) distances, capturing significant geometric errors, to evaluate the accuracy of the reconstructed meshes. We assess the quality of local details and the efficacy of 3D features via the L2 error between normal images of reconstructed and ground-truth meshes from six views. Finally, the quality of texture prediction is measured using Peak Signal-to-Noise Ratio (PSNR), comparing images rendered from both reconstructed and ground-truth surfaces across different views.

4.1 Evaluation

Evaluation of Geometry. We compare our **GTA** model with body-agnostic methods like PIFu [1], PIFuHD [6], and body-aware methods such as PaMIR [3], ICON [2], and ECON [4]. Our evaluation is thorough, involving training and testing these models ourselves and incorporating testing results from [4, 2] for a comprehensive comparison. As depicted in Tab. 1, **GTA** excels in terms of Chamfer and P2S distances on images with out-of-distribution (OOD) poses and diverse clothing. Notably, **GTA** is the first to reduce the Chamfer distance to less than 0.8 cm on CAPE-FP. On par with ECON for normals on CAPE, **GTA** sets a new state-of-the-art on THuman2.0. Fig. 8a visually underlines our model’s superior performance on the THuman2.0 benchmarks.

Quantitative Evaluation of Side-face Reconstruction. In our novel quantitative evaluation of side-face reconstruction, we spotlight the advantages of 3D features in crafting plausible side-faces and accurate thickness. Using six virtual camera angles, we render normal images of the reconstructed human and compute the normal difference for each face on the THuman2.0 [15] dataset. As shown in Tab. 2, **GTA** surpasses other models in 5 out of 6 views, matching ECON only in the front view, thereby underscoring our model’s prowess in capturing inherent 3D structures within an image. For visual results, refer to Fig. 2 and Fig. 11a.

Evaluation of Texture. In evaluating texture reconstruction, we compare **GTA** with color-predicting models like PIFu [1], ARCH [8], ARCH++ [9], PHORHUM [5], and S3F [7]. By rendering textured meshes from multiple angles and calculating the PSNR with respect to ground truth images, we find **GTA** outperforms other models on THuman2.0. As Fig. 5 demonstrates, **GTA** exceeds the state-of-the-art S3F [7] by 22% in PSNR. Notably, our model provides superior textures on the front side and accurately predicts invisible regions, as seen in Fig. 8b, highlighting the effectiveness of 3D features.

4.2 Ablation Study

Ablation Details. To ensure a fair and unbiased experimental setup, we employed an approach wherein the implicit functions of each ablation experiment were augmented with front and back

Table 2: Normal Evaluation of Different Views on THuman2.0 [15]. These views are obtained by positioning a virtual camera at the front, left, back, right, above, and below the reconstructed human.

Method	Normals of Different Views						Average
	Front	Left	Back	Right	Above	Below	
PIFu [1]	0.053	0.143	0.046	0.109	0.067	0.066	0.081
PaMIR [3]	0.051	0.124	0.068	0.077	0.051	0.054	0.071
ICON [2]	0.074	0.091	0.0647	0.076	0.044	0.044	0.066
ECON [4]	0.043	0.123	<u>0.045</u>	0.083	0.050	<u>0.041</u>	<u>0.064</u>
Ours	<u>0.048</u>	0.069	0.044	0.061	0.035	0.040	0.050



Figure 5: Quantitative Evaluation of Texture on THuman2.0 [15].

Table 3: Ablation study of several of our designs on CAPE [16] dataset.

(a) Different networks.			(b) 2D features vs. 3D features.			(c) Different query methods.					
Method	Chamfer↓	P2S↓	Normals↓	Method	Chamfer↓	P2S↓	Normals↓	Method	Chamfer↓	P2S↓	Normals↓
use convolution	0.991	0.968	0.055	2D+SQ	1.054	1.052	0.054	3D+SQ	0.987	0.965	0.049
w/o cross-atten	0.937	0.922	0.051	2D+PQ	1.133	1.116	0.053	3D+PQ	1.059	0.987	0.048
w/o refine	0.890	0.882	0.053	2D+hybrid	1.008	0.967	0.051	Ours	0.861	0.866	0.045
Ours	0.861	0.866	0.045	Ours	0.861	0.866	0.045				



Figure 6: Texture change of different ablation settings.



Figure 7: Application of our model in animation and virtual try-on.

normal features and signed distances from the human prior body. For the ablation experiments pertaining to different network architectures, we replaced the corresponding components of our network structure with three identical UNet [53] and Vision Transformer [41] decoders solely based on self-attention, respectively. Moreover, for the ablations on 2D features, we generated a 2D feature map of size 256×256 with UNet. Additionally, for the ablations on the hybrid prior fusion strategy, we employed a single tri-plane for the spacial query and the prior-enhanced query, respectively.

A. Different Networks for 3D Feature Decoupling. We evaluate alternative architectures by modifying our global-correlated encoder and 3D-decoupling decoder, confirming the strength of our proposed transformer. We experiment with UNet [53], also used in [7], as a convolution filter representative, and employ three separate UNets to compose the tri-plane. We also test a transformer encoder-decoder with only self-attention and without the refinement module or additional learnable embeddings. Results (see Tab. 3 and Fig. 6) suggest that a purely convolution-based network struggles to decouple 3D features due to limited correlation and receptive field constraints. While the refinement module shows minor geometric improvements, it is crucial for texture reconstruction. Additional learnable embeddings and cross-attention blocks notably enhance geometry results.

B. 2D Features vs. 3D Features. We analyze the effectiveness of 3D features by conducting an ablation study using solely 2D feature maps for reconstruction. Utilizing UNet [53] to generate high-dimensional 2D features, we compare spatial query (SQ), prior-enhanced query (PQ), and our hybrid prior fusion strategy. Results highlight the inferiority of 2D features in producing accurate reconstructions (Tab. 3), emphasizing the importance of 3D features.

C. Hybrid Prior Fusion Strategy vs. Others. We evaluate our hybrid prior fusion strategy against individual use of spatial query (SQ) and prior-enhanced query (PQ). Results show that spatial query surpasses prior-enhanced query in both geometry and texture quality due to its provision of localized features for detailed reconstruction. However, combining both methods optimizes geometry performance while preserving texture quality, demonstrating the effectiveness of our hybrid strategy.

4.3 Applications

Reconstruction of Images in-the-wild. The GTA model demonstrates significant prowess in reconstructing 3D human meshes from unconstrained, real-world images (refer to Fig. 4 and Fig. 12), addressing the complexities posed by varied poses and clothing styles. This capability of recon-

structing high-fidelity 3D models from in-the-wild images paves the way for extensive applications, notably in virtual and augmented reality.

Animation and Virtual Try-On. We present a robust approach for generating novel poses of 3D clothed human meshes, catering to applications in animation and virtual try-on (See Fig. 7). We extend the S3F [7] model by employing estimated body shape and pose parameters to derive tri-plane features, facilitating realistic deformations. For a single-image clothed human reconstruction, our method excels by only needing the target pose, thus overcoming the limitations of previous deep learning methods. Additionally, our model supports virtual try-on by enabling feature replacement across body parts of different parametric bodies. By selectively interchanging these features, we can simulate changes in clothing on the target image. Our method, therefore, provides a versatile solution for both animation and virtual try-on applications, merging the strengths of previous methods while alleviating their weaknesses. More technical details and results are available in Sec. A and E.

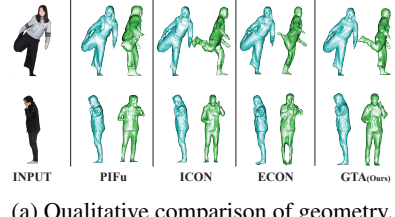
5 Conclusion

In conclusion, we present the **GTA** model, a cutting-edge approach for reconstructing 3D clothed human from single images. Our global-correlated 3D-decoupling transformer effectively extracts latent representations from input images and integrates them with learnable embeddings through 3D-decoupling decoders, generating disentangled tri-plane features. Moreover, our hybrid prior fusion strategy integrates the benefits of spatial query’s localization capabilities with the prior-enhanced query’s ability to incorporate knowledge of the human body prior, ultimately leading to improved geometry and texture reconstruction performance. We demonstrate that our proposed model outperforms state-of-the-art methods in geometric and texture reconstruction, exhibiting resilience against challenging poses and loose clothing, enabling a wide range of applications.

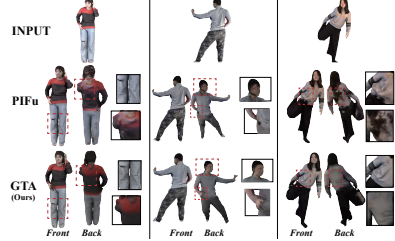
Acknowledgements. This work was supported in part by the Fundamental Research Funds for the Central Universities (No. 226-2023-00048) and the Natural Science Foundation of Zhejiang Province (DT23F020008).

References

- [1] Shunsuke Saito, Zeng Huang, Ryota Natsume, Shigeo Morishima, Angjoo Kanazawa, and Hao Li. Pifu: Pixel-aligned implicit function for high-resolution clothed human digitization. In *The IEEE International Conference on Computer Vision (ICCV)*, October 2019.
- [2] Yuliang Xiu, Jinlong Yang, Dimitrios Tzionas, and Michael J. Black. ICON: Implicit Clothed humans Obtained from Normals. In *Proceedings of the IEEE/CVF Conference on Computer Vision and Pattern Recognition (CVPR)*, pages 13296–13306, June 2022.
- [3] Zerong Zheng, Tao Yu, Yebin Liu, and Qionghai Dai. Pamir: Parametric model-conditioned implicit representation for image-based human reconstruction. *IEEE transactions on pattern analysis and machine intelligence*, 44(6):3170–3184, 2021.
- [4] Yuliang Xiu, Jinlong Yang, Xu Cao, Dimitrios Tzionas, and Michael J. Black. ECON: Explicit Clothed humans Optimized via Normal integration. In *Proceedings of the IEEE/CVF Conference on Computer Vision and Pattern Recognition (CVPR)*, June 2023.
- [5] Thieno Alldieck, Mihai Zanfir, and Cristian Sminchisescu. Photorealistic monocular 3d reconstruction of humans wearing clothing. In *Proceedings of the IEEE/CVF Conference on Computer Vision and Pattern Recognition*, pages 1506–1515, 2022.
- [6] Shunsuke Saito, Tomas Simon, Jason Saragih, and Hanbyul Joo. Pifuhd: Multi-level pixel-aligned implicit function for high-resolution 3d human digitization. In *CVPR*, 2020.



(a) Qualitative comparison of geometry.



(b) Qualitative comparison of texture.

Figure 8: Comparison of geometry and texture on THuman2.0 [15] benchmark.

- [7] Enric Corona, Mihai Zanfir, Thiemo Alldieck, Eduard Gabriel Bazavan, Andrei Zanfir, and Cristian Sminchisescu. Structured 3d features for reconstructing relightable and animatable avatars. *arXiv preprint arXiv:2212.06820*, 2022.
- [8] Zeng Huang, Yuanlu Xu, Christoph Lassner, Hao Li, and Tony Tung. Arch: Animatable reconstruction of clothed humans. In *Proceedings of the IEEE/CVF Conference on Computer Vision and Pattern Recognition*, pages 3093–3102, 2020.
- [9] Tong He, Yuanlu Xu, Shunsuke Saito, Stefano Soatto, and Tony Tung. Arch++: Animation-ready clothed human reconstruction revisited. In *Proceedings of the IEEE/CVF international conference on computer vision*, pages 11046–11056, 2021.
- [10] Yukang Cao, Kai Han, and Kwan-Yee K. Wong. Sesdf: Self-evolved signed distance field for implicit 3d clothed human reconstruction. In *IEEE Conference on Computer Vision and Pattern Recognition (CVPR)*, 2023.
- [11] Valentin Gabeur, Jean-Sébastien Franco, Xavier Martin, Cordelia Schmid, and Gregory Rogez. Moulding humans: Non-parametric 3d human shape estimation from single images. In *Proceedings of the IEEE/CVF international conference on computer vision*, pages 2232–2241, 2019.
- [12] David Smith, Matthew Loper, Xiaochen Hu, Paris Mavroidis, and Javier Romero. Facsimile: Fast and accurate scans from an image in less than a second. In *Proceedings of the IEEE/CVF international conference on computer vision*, pages 5330–5339, 2019.
- [13] Yongqin Xian, Julian Chibane, Bharat Lal Bhatnagar, Bernt Schiele, Zeynep Akata, and Gerard Pons-Moll. Any-shot gin: Generalizing implicit networks for reconstructing novel classes. In *2022 International Conference on 3D Vision (3DV)*, pages 526–535. IEEE, 2022.
- [14] Eric R. Chan, Connor Z. Lin, Matthew A. Chan, Koki Nagano, Boxiao Pan, Shalini De Mello, Orazio Gallo, Leonidas Guibas, Jonathan Tremblay, Sameh Khamis, Tero Karras, and Gordon Wetzstein. Efficient geometry-aware 3D generative adversarial networks. In *CVPR*, 2022.
- [15] Tao Yu, Zerong Zheng, Kaiwen Guo, Pengpeng Liu, Qionghai Dai, and Yebin Liu. Function4d: Real-time human volumetric capture from very sparse consumer rgbd sensors. In *IEEE Conference on Computer Vision and Pattern Recognition (CVPR2021)*, June 2021.
- [16] Qianli Ma, Jinlong Yang, Anurag Ranjan, Sergi Pujades, Gerard Pons-Moll, Siyu Tang, and Michael J. Black. Learning to Dress 3D People in Generative Clothing. In *Computer Vision and Pattern Recognition (CVPR)*, June 2020.
- [17] Dragomir Anguelov, Praveen Srinivasan, Daphne Koller, Sebastian Thrun, Jim Rodgers, and James Davis. Scape: shape completion and animation of people. In *ACM SIGGRAPH 2005 Papers*, pages 408–416. ACM, 2005.
- [18] Matthew Loper, Naureen Mahmood, Javier Romero, Gerard Pons-Moll, and Michael J Black. Smpl: A skinned multi-person linear model. *ACM transactions on graphics (TOG)*, 34(6):1–16, 2015.
- [19] Georgios Pavlakos, Vasileios Choutas, Nima Ghorbani, Timo Bolkart, Ahmed A. A. Osman, Dimitrios Tzionas, and Michael J. Black. Expressive body capture: 3D hands, face, and body from a single image. In *Proceedings IEEE Conf. on Computer Vision and Pattern Recognition (CVPR)*, pages 10975–10985, 2019.
- [20] Ahmed AA Osman, Timo Bolkart, and Michael J Black. Star: Sparse trained articulated human body regressor. In *Computer Vision–ECCV 2020: 16th European Conference, Glasgow, UK, August 23–28, 2020, Proceedings, Part VI 16*, pages 598–613. Springer, 2020.
- [21] Hongyi Xu, Eduard Gabriel Bazavan, Andrei Zanfir, William T Freeman, Rahul Sukthankar, and Cristian Sminchisescu. Ghum & ghuml: Generative 3d human shape and articulated pose models. In *Proceedings of the IEEE/CVF Conference on Computer Vision and Pattern Recognition*, pages 6184–6193, 2020.
- [22] Federica Bogo, Angjoo Kanazawa, Christoph Lassner, Peter Gehler, Javier Romero, and Michael J. Black. Keep it SMPL: Automatic estimation of 3D human pose and shape from a single image. In *Computer Vision – ECCV 2016*, Lecture Notes in Computer Science. Springer International Publishing, October 2016.
- [23] Angjoo Kanazawa, Michael J. Black, David W. Jacobs, and Jitendra Malik. End-to-end recovery of human shape and pose. In *Computer Vision and Pattern Recognition (CVPR)*, 2018.

[24] Muhammed Kocabas, Chun-Hao P. Huang, Otmar Hilliges, and Michael J. Black. PARE: Part attention regressor for 3D human body estimation. In *Proc. International Conference on Computer Vision (ICCV)*, pages 11127–11137, October 2021.

[25] Hongwen Zhang, Yating Tian, Xinchi Zhou, Wanli Ouyang, Yebin Liu, Limin Wang, and Zhenan Sun. Pymaf: 3d human pose and shape regression with pyramidal mesh alignment feedback loop. In *Proceedings of the IEEE/CVF International Conference on Computer Vision*, pages 11446–11456, 2021.

[26] Yao Feng, Vasileios Choutas, Timo Bolkart, Dimitrios Tzionas, and Michael J Black. Collaborative regression of expressive bodies using moderation. In *2021 International Conference on 3D Vision (3DV)*, pages 792–804. IEEE, 2021.

[27] Thiemo Alldieck, Marcus Magnor, Bharat Lal Bhatnagar, Christian Theobalt, and Gerard Pons-Moll. Learning to reconstruct people in clothing from a single rgb camera. In *Proceedings of the IEEE/CVF Conference on Computer Vision and Pattern Recognition*, pages 1175–1186, 2019.

[28] Thiemo Alldieck, Marcus Magnor, Weipeng Xu, Christian Theobalt, and Gerard Pons-Moll. Detailed human avatars from monocular video. In *2018 International Conference on 3D Vision (3DV)*, pages 98–109. IEEE, 2018.

[29] Thiemo Alldieck, Marcus Magnor, Weipeng Xu, Christian Theobalt, and Gerard Pons-Moll. Video based reconstruction of 3d people models. In *Proceedings of the IEEE Conference on Computer Vision and Pattern Recognition*, pages 8387–8397, 2018.

[30] Thiemo Alldieck, Gerard Pons-Moll, Christian Theobalt, and Marcus Magnor. Tex2shape: Detailed full human body geometry from a single image. In *Proceedings of the IEEE/CVF International Conference on Computer Vision*, pages 2293–2303, 2019.

[31] Hao Zhu, Xinxin Zuo, Sen Wang, Xun Cao, and Ruigang Yang. Detailed human shape estimation from a single image by hierarchical mesh deformation. In *Proceedings of the IEEE/CVF conference on computer vision and pattern recognition*, pages 4491–4500, 2019.

[32] Gul Varol, Duygu Ceylan, Bryan Russell, Jimei Yang, Ersin Yumer, Ivan Laptev, and Cordelia Schmid. Bodynet: Volumetric inference of 3d human body shapes. In *Proceedings of the European conference on computer vision (ECCV)*, pages 20–36, 2018.

[33] Zerong Zheng, Tao Yu, Yixuan Wei, Qionghai Dai, and Yebin Liu. Deephuman: 3d human reconstruction from a single image. In *Proceedings of the IEEE/CVF International Conference on Computer Vision*, pages 7739–7749, 2019.

[34] Ryota Natsume, Shunsuke Saito, Zeng Huang, Weikai Chen, Chongyang Ma, Hao Li, and Shigeo Morishima. Siclope: Silhouette-based clothed people. In *Proceedings of the IEEE/CVF Conference on Computer Vision and Pattern Recognition*, pages 4480–4490, 2019.

[35] Albert Pumarola, Jordi Sanchez-Riera, Gary Choi, Alberto Sanfeliu, and Francesc Moreno-Noguer. 3dpeople: Modeling the geometry of dressed humans. In *Proceedings of the IEEE/CVF international conference on computer vision*, pages 2242–2251, 2019.

[36] Zhiqin Chen and Hao Zhang. Learning implicit fields for generative shape modeling. In *Proceedings of the IEEE/CVF Conference on Computer Vision and Pattern Recognition*, pages 5939–5948, 2019.

[37] Jeong Joon Park, Peter Florence, Julian Straub, Richard Newcombe, and Steven Lovegrove. Deepsdf: Learning continuous signed distance functions for shape representation. In *Proceedings of the IEEE/CVF conference on computer vision and pattern recognition*, pages 165–174, 2019.

[38] Lars Mescheder, Michael Oechsle, Michael Niemeyer, Sebastian Nowozin, and Andreas Geiger. Occupancy networks: Learning 3d reconstruction in function space. In *Proceedings of the IEEE/CVF conference on computer vision and pattern recognition*, pages 4460–4470, 2019.

[39] Tong He, John Collomosse, Hailin Jin, and Stefano Soatto. Geo-pifu: Geometry and pixel aligned implicit functions for single-view human reconstruction. *Advances in Neural Information Processing Systems*, 33:9276–9287, 2020.

[40] Ashish Vaswani, Noam Shazeer, Niki Parmar, Jakob Uszkoreit, Llion Jones, Aidan N Gomez, Łukasz Kaiser, and Illia Polosukhin. Attention is all you need. *Advances in neural information processing systems*, 30, 2017.

[41] Alexey Dosovitskiy, Lucas Beyer, Alexander Kolesnikov, Dirk Weissenborn, Xiaohua Zhai, Thomas Unterthiner, Mostafa Dehghani, Matthias Minderer, Georg Heigold, Sylvain Gelly, et al. An image is worth 16x16 words: Transformers for image recognition at scale. *arXiv preprint arXiv:2010.11929*, 2020.

[42] Jun Gao, Tianchang Shen, Zian Wang, Wenzheng Chen, Kangxue Yin, Daiqing Li, Or Litany, Zan Gojcic, and Sanja Fidler. Get3d: A generative model of high quality 3d textured shapes learned from images. *Advances In Neural Information Processing Systems*, 35:31841–31854, 2022.

[43] Atsuhiro Noguchi, Xiao Sun, Stephen Lin, and Tatsuya Harada. Unsupervised learning of efficient geometry-aware neural articulated representations. In *Computer Vision–ECCV 2022: 17th European Conference, Tel Aviv, Israel, October 23–27, 2022, Proceedings, Part XVII*, pages 597–614. Springer, 2022.

[44] Alexander Bergman, Petr Kellnhofer, Wang Yifan, Eric Chan, David Lindell, and Gordon Wetzstein. Generative neural articulated radiance fields. *Advances in Neural Information Processing Systems*, 35:19900–19916, 2022.

[45] Suyi Jiang, Haoran Jiang, Ziyu Wang, Haimin Luo, Wenzheng Chen, and Lan Xu. Humangen: Generating human radiance fields with explicit priors. *arXiv preprint arXiv:2212.05321*, 2022.

[46] Kaiming He, Xiangyu Zhang, Shaoqing Ren, and Jian Sun. Deep residual learning for image recognition. In *Proceedings of the IEEE conference on computer vision and pattern recognition*, pages 770–778, 2016.

[47] Jimmy Lei Ba, Jamie Ryan Kiros, and Geoffrey E Hinton. Layer normalization. *arXiv preprint arXiv:1607.06450*, 2016.

[48] Renderpeople. <https://renderpeople.com/>.

[49] Clement Fuji Tsang, Maria Shugrina, Jean Francois Lafleche, Towaki Takikawa, Jiehan Wang, Charles Loop, Wenzheng Chen, Krishna Murthy Jatavallabhula, Edward Smith, Artem Rozantsev, Or Perel, Tianchang Shen, Jun Gao, Sanja Fidler, Gavriel State, Jason Gorski, Tommy Xiang, Jianing Li, Michael Li, and Rev Lebaredian. Kaolin: A pytorch library for accelerating 3d deep learning research. <https://github.com/NVIDIAAGameWorks/kaolin>, 2022.

[50] Daniel Gatis. Rembg: A tool to remove images background. <https://github.com/danielgatis/rembg>, 2022.

[51] William E Lorensen and Harvey E Cline. Marching cubes: A high resolution 3d surface construction algorithm. *ACM siggraph computer graphics*, 21(4):163–169, 1987.

[52] William Falcon and The PyTorch Lightning team. PyTorch Lightning, 2019.

[53] Olaf Ronneberger, Philipp Fischer, and Thomas Brox. U-net: Convolutional networks for biomedical image segmentation. In *Medical Image Computing and Computer-Assisted Intervention–MICCAI 2015: 18th International Conference, Munich, Germany, October 5–9, 2015, Proceedings, Part III 18*, pages 234–241. Springer, 2015.

[54] Rui long Li, Shan Yang, David A. Ross, and Angjoo Kanazawa. Learn to dance with aist++: Music conditioned 3d dance generation, 2021.

[55] Leif E Peterson. K-nearest neighbor. *Scholarpedia*, 4(2):1883, 2009.

[56] Tao Ju, Scott Schaefer, and Joe Warren. Mean value coordinates for closed triangular meshes. In *ACM Siggraph 2005 Papers*, pages 561–566. 2005.

[57] Zhe Li, Zerong Zheng, Hongwen Zhang, Chaonan Ji, and Yebin Liu. Avatarcap: Animatable avatar conditioned monocular human volumetric capture. In *European Conference on Computer Vision (ECCV)*, October 2022.

[58] Shunsuke Saito, Jinlong Yang, Qianli Ma, and Michael J. Black. SCANimate: Weakly supervised learning of skinned clothed avatar networks. In *Proceedings IEEE/CVF Conf. on Computer Vision and Pattern Recognition (CVPR)*, June 2021.

[59] Qianli Ma, Jinlong Yang, Siyu Tang, and Michael J. Black. The power of points for modeling humans in clothing. In *Proceedings of the IEEE/CVF International Conference on Computer Vision (ICCV)*, October 2021.

- [60] Qianli Ma, Shunsuke Saito, Jinlong Yang, Siyu Tang, and Michael J. Black. SCALE: Modeling clothed humans with a surface codec of articulated local elements. In *Proceedings IEEE/CVF Conf. on Computer Vision and Pattern Recognition (CVPR)*, pages 16082–16093, 2021.
- [61] Jianglin Fu, Shikai Li, Yuming Jiang, Kwan-Yee Lin, Chen Qian, Chen-Change Loy, Wayne Wu, and Ziwei Liu. Stylegan-human: A data-centric odyssey of human generation. *arXiv preprint*, arXiv:2204.11823, 2022.
- [62] Ziwei Liu, Ping Luo, Shi Qiu, Xiaogang Wang, and Xiaoou Tang. Deepfashion: Powering robust clothes recognition and retrieval with rich annotations. In *Proceedings of IEEE Conference on Computer Vision and Pattern Recognition (CVPR)*, June 2016.

A Implementation Details

Estimation of Prior. For the initial estimation of the human body, we resort to the utilization of either the SMPL-X model, as outlined in PIXIE [26], or the SMPL model, as delineated in PyMAF [25]. A variety of motion datasets like AIST++ [54] adopt SMPL parameters for animation representation, and hence we have used SMPL as the prior in the results depicted in Fig. 13.

During the training phase, the SMPL-X data tailored for THuman2.0 [15] is used as the human prior. For our geometry testing with open-source models, as delineated in Tab. 1, we utilized the ground-truth SMPL/SMPL-X, consistent with the methodologies employed by ICON [2] and ECON [4]. In the texture performance evaluations with non-public models, such as S3F [7] in Fig. 5, we abstained from using ground-truth SMPL and instead leveraged PyMAF [25] to derive the SMPL prior. While during the inference stage, we employ the readily available models [26, 25] to predict parameters for the human prior. In order to bolster the precision of the reconstructed outcomes, we deploy the refinement technique from [2], which allows us to optimize the SMPL/SMPL-X parameters for a reduced silhouette loss.

Prior-guided Tri-plane Deformation. Previous methods for generating novel poses of 3D clothed human meshes can be grouped into two categories. The first binds the 3D mesh with a human body prior, using algorithms like KNN [55], Surface Field [44], and MVC [56]. However, this approach has limited robustness and may cause distorted deformations in self-intersecting parts of the model. The second category employs deep learning to predict blend weights for each mesh point, enabling more realistic movements. These methods [57, 58, 59, 60] often require training on multiple 3D meshes of the same person in different poses, posing challenges for single-image clothed human reconstruction. Motivated by the S3F [7] approach, we employ the estimated body shape and pose parameters, denoted as β and θ , to obtain tri-plane features and transfer the features of each vertex in the prior model $\mathcal{M}(\beta, \theta)$ to the corresponding vertex in the posed prior $\mathcal{M}'(\beta, \theta')$, where θ' represents the target pose. Subsequently, we use barycentric interpolation to obtain the feature and feed them into the MLP to predict the 3D mesh and texture in the new pose.

Virtual Try-on. In our model, we can partition 3D features based on body parts (e.g., left arm, right leg) once integrated into a parametric human body. Given a reference and a target image, we feed them into our model to obtain two parametric bodies with vertex-specific features. We can then replace features on the target body’s selected part (where clothes change is desired) with the corresponding features from the reference body. This replacement allows the target image’s query point to acquire reference image features, enabling the implicit function to output colors from the reference image on the replaced parts.

B Experiments Analysis

We further analyze our experimental results and provide corresponding theoretical explanations.

Regarding quantitative evaluation metrics for geometry reconstruction, we observed that our approach achieved significant improvement in terms of Chamfer Distance and Point-to-Surface metrics, especially for in-distribution poses. The predominant factor of these advancements lies in our consideration of features of the orthogonal planes during reconstruction. Firstly, both of these metrics are employed to assess the large geometric differences. As exemplified by the results presented in Fig. 11a, ECON tends to exhibit larger errors in the orthogonal planes compared to GTA. These orthogonal plane errors manifest in three-dimensional space as overall surface shifts, significantly influencing chamfer distance and P2S metrics. Moreover, in terms of normal consistency, as ECON [4] explicitly integrates both front and back normal maps and performs explicit stitching for better hands and face details, our method yielded slightly lower results than ECON in the case of the CAPE [16] dataset. Conversely, in more intricate datasets like THuman2.0 [15], characterized by complexity and substantial occlusions, the disparities in the normal maps are pronounced, resulting in GTA exhibiting better overall Normals. In our further assessment of normal consistency, we observed that ECON [4] surpassed our method in

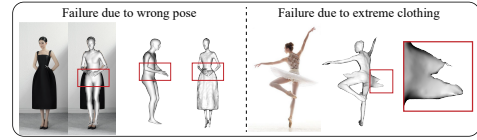


Figure 9: Failure cases. Inaccurate results due to incorrect human prior estimation (left) and failure cases due to extreme clothing (right).

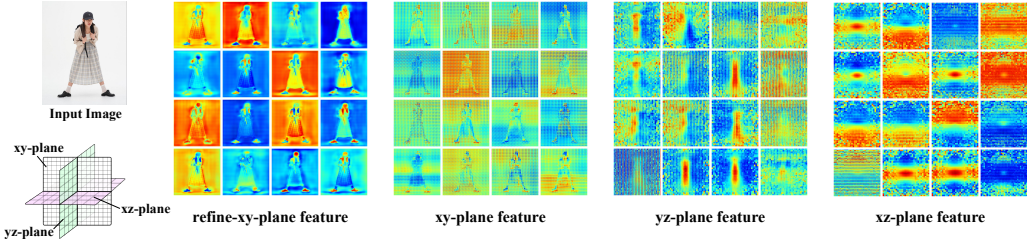


Figure 10: Tri-plane feature map visualization. The graphical display highlights the first 16 channels of our decoupled tri-plane features. These features effectively capture the human body’s silhouette, demonstrating effectiveness of our approach.

terms of front view, which aligned with our analysis. For other views, our model produced rendered normal maps that more closely approximated the ground truth due to the utilization of our 3D features.

The qualitative results of texture exhibit our method’s superior performance in predicting textures of invisible regions. We attribute this success to our extraction of decoupled 3D features. Additionally, we conducted comprehensive ablation experiments, which provided evidence for the effectiveness of our network architecture, decoupled 3D features, and hybrid prior fusion strategy. Specifically, the results of the ablation experiments demonstrated that our network architecture, tri-plane features, and hybrid prior fusion strategy played indispensable roles in geometry reconstruction. Besides, the reconstruction of texture was primarily influenced by the principle plane refinement and spatial query.

C Limitations

Our method exhibits robust performance in general, though it does face challenges under certain circumstances, as depicted in Fig. 9. The model relies on pre-existing models [26, 25] to deduce a SMPL [18] or SMPL-X [19] from a single RGB image, thus errors in estimations can consequently affect our reconstruction. Additionally, our model faces difficulties with extremely loose clothing that considerably deviates from the human body’s contours. To address these issues, future research could explore the integration of more explicit information during the reconstruction phase.

D Broader Impacts

Our model’s ability to reconstruct 3D realistic avatars from single input images raises potential negative impacts, including privacy violations, "deep fakes" generation, and intellectual property infringement. To address these concerns, ethical guidelines and legal frameworks must be established, requiring collaboration among researchers, developers, and policymakers to ensure responsible applications of this technology.

E Additional Results

To further demonstrate the effectiveness of GTA, we compared it with the state-of-the-art methods in terms of time and space occupancy. In Tab. 4a, it’s evident that our model outperforms the UNet-based approach with fewer parameters, as indicated by better reconstruction results. This highlights the advantages of our transformer-based design in extracting 3D features. Tab. 4b displays the comparable time efficiency of our implicit function-based model with PIFu, Pamir, and ICON. In contrast, ECON, relying on explicit methods, demands more time due to d-BiNI and Poisson inefficiencies. CAPE-NFP dataset with 256^3 resolution is used for testing, ground truth SMPL/SMPL-X provided.

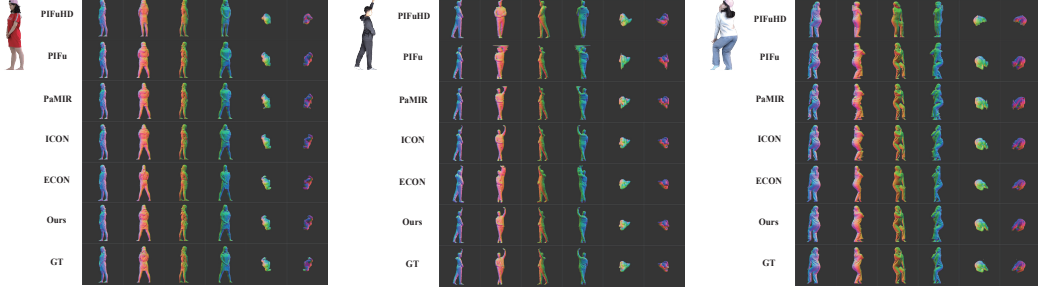
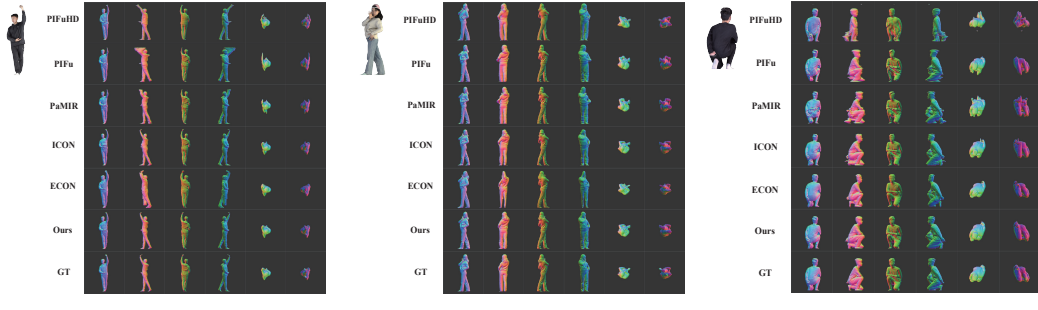
In order to assess the effectiveness of the decoupled tri-plane features, we conducted a visual analysis of the first 16 channels of these features in Fig. 10. The visualizations demonstrated that our refined principle plane features exhibited higher resolution and better visual results. While the features of the orthogonal planes appeared blurred, they still captured the overall outline of the human body. This observation serves as empirical evidence of the effectiveness of our approach, which incorporates 3D-decoupling decoders and principle plane refinement.

Table 4: Comparison of parameters and inference time.

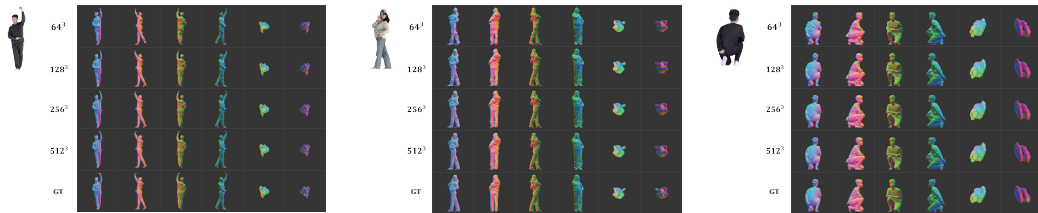
(a) Parameter number comparison.			(b) Inference time of different SOTA models.					
Method	use convolution	ours	Method	PIFu	Pamir	ICON	ECON	GTA
Total params	93,135,264	36,977,056	Inference time (s)	0.37	0.44	0.37	15.07	0.55

Fig. 11 compares the qualitative reconstruction results for geometry between the GTA and SOTA methods and showcases the impact of marching cubes resolution on GTA. In Fig. 11a, we provide rendered normal maps under the setting of quantitative testing (resolution of 256). The reconstruction results are rendered as normal maps from six different viewing angles. The results demonstrate that our approach is comparable to the SOTA methods for front-face reconstruction and outperforms them for side-face reconstruction. These qualitative results are consistent with the quantitative experiments presented in the main text and our analysis in the last section. In Fig. 11b, we illustrate various resolutions’ effects on GTA’s reconstruction results, elucidating the causes of detail loss.

Next, we build upon the results elucidated in the main paper by furnishing additional qualitative outcomes for various tasks. We present an extended range of monocular 3D clothed human reconstruction results in Fig. 12, demonstrating a wide assortment of input conditions in terms of poses, backgrounds, viewpoints, and clothing. Further, we showcase supplementary results of 3D human animation in Fig. 13 and 3D virtual try-on in Fig. 14 using images from Pinterest, SHHQ [61], and Deep Fashion [62]. While the animation and virtual try-on results offer a compelling demonstration of our model’s capability, it’s important to acknowledge that the resolution of these results does not quite match that of the reconstructed outcomes. This minor discrepancy arises from our approach that relies exclusively on the prior-enhanced query for these two applications. Although the current version of the spatial query cannot ensure smooth point deformation for these applications, which may cause minor artifacts, this represents a valuable avenue for potential improvement in future iterations. Nevertheless, the results of these two applications remain competitive when compared with other state-of-the-art methods.



(a) Qualitative comparison of geometry.



(b) Qualitative comparison of different marching cube resolution.

Figure 11: Comparison of geometry on THuman2.0 benchmark. Please zoom in for details.



Figure 12: Qualitative 3D human reconstruction results on in-the-wild images with geometry and texture. For each example, we show the input image along with two views (front and back) of the reconstructed geometry and two views (front and back) of the reconstructed texture. Our approach is robust to pose variations, generalizes well to loose clothing, and contains detailed geometry and texture. Please zoom in for details.



Figure 13: Qualitative results on animation of 3D reconstructions.

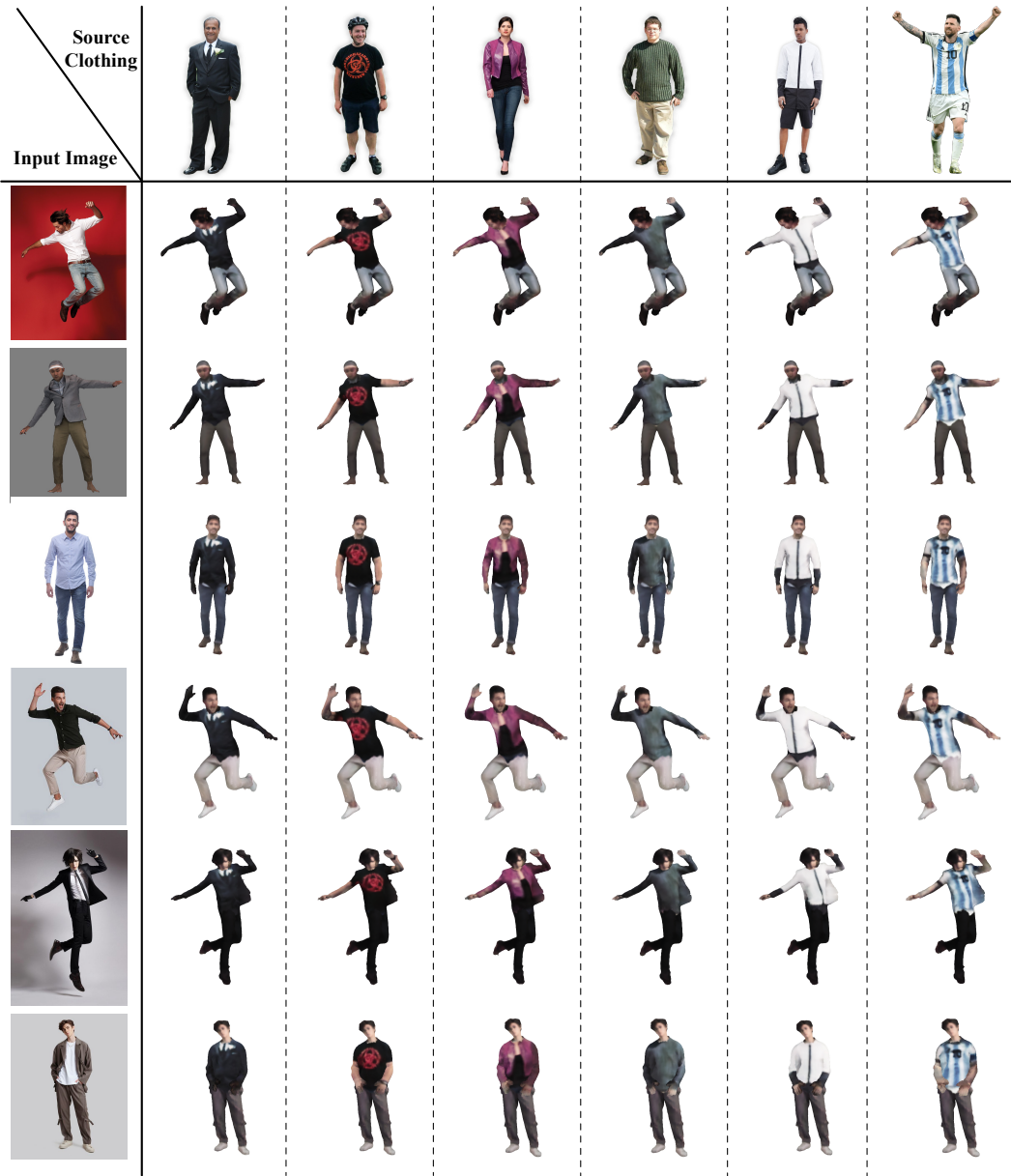


Figure 14: Qualitative results of 3D virtual try-on. We broaden the scope of the experiment discussed in the main paper by demonstrating an instance of upper-body clothing try-on and present both the input images (left) and source clothing (upper row). The 3D reconstructions generated exhibit high realism and consistency across all samples.